Restoration of the Salton Sea

Volume 1: Evaluation of the Alternatives

Appendix 1I: One-Dimensional Hydrodynamic and Thermodynamic Modeling of a Modified Salton Sea under Future Inflow Conditions

Contents

Page

Tables

Figures

Executive Summary

ONE-DIMENSIONAL HYDRODYNAMIC AND THERMODYNAMIC MODELING OF A MODIFIED SALTON SEA UNDER FUTURE INFLOW CONDITIONS

S.G. Schladow, University of California-Davis

A one-dimensional hydrodynamic and thermodynamic model has been modified to evaluate the types of changes to the Salton Sea that might arise under scenarios that are currently under consideration by Reclamation. This model was the basis of DLM-WQ which was recently used to model the eutrophic state of the current Salton Sea on behalf of the Regional Water Quality Control Board. The extent of thermal stratification allows informed decisions about the likelihood and extent of hypoxia, H_2S and NH_4 formation.

A Base Case was initially run for a one year period using data from 1999 in order to determine that it matched the available measurements. CIMIS meteorological data were used to drive the model. The Base Case condition used the measured average annual discharges. These were 620,000 acre-ft from Alamo River, 438,000 acre-ft from New River, 79,000 acre-ft from the Whitewater River and 106,000 acre-ft from agricultural drains. The initial conditions were set based on measurements by Holdren. The results showed good agreement with the 12 months of measurements, characterized by stratification over an approximately 4 month period. The stratification was weak, broke and reformed several times, and was dominated by a broad thermocline. This is suggestive of the domination of shear mixing associated with seiching, a process that would allow periodic venting of hypolimnetic water.

Two sets of simulations were run to examine the Sea's response under modified flow conditions. In both sets of simulations, the inflow to the Sea was assumed to be 800,000 ac-ft, evenly divided between the New and Alamo Rivers. In the first set of simulations, the geometry of the Sea was preserved, but the initial water depth was altered. The 5 depths considered were 14.9 m, 14 m, 12 m, 10 m and 8 m. The results indicated that the 14.9 m and 14 m cases produced similar results. However for 12 m depth, only a very weak and short stratification period persisted. For the 10 m and 8 m cases, thermal stratification was virtually eliminated throughout the year. This implies that there would be very limited episodes of hypoxia and the production of H_2S and NH_4 for full Sea depths below

10-12 m. Model runs assuming a higher clarity Sea (i.e., less eutrophication) showed that stratification was reduced for the deeper Sea scenarios (14.9 m, 14 m and 12 m). The occurrence of cold water days was also examined for each water depth (due to the impact on tilapia survival over winter). For the 14.9 m and 14 m depths, there were no days with water temperatures below 12°C. Between 12 m and 8 m, the number of days with water temperatures below 10°C increased from approximately 15 to 25 days.

In the second set of simulations, the effect of dividing the Sea with a dam or barrier was explored. This was done by reducing the lake volume by 50% at all depths. While particular Reclamation scenarios are a little different than this, the difference to the physics of the Sea is expected to be small. The results are expected to be similar whether the remnant Sea was in the north or the south. A maximum Sea depth of 14 m was used for this set of simulations, assuming that the existing shoreline would be preserved.

The effect of halving the area of the Sea was dramatic. Thermal stratification was intensified, with the formation of a very sharp and intense thermocline commencing at a depth of about 4 m below the surface. The stratification was also extremely persistent, with all but 1-2 months being stratified. The breakdown of stratification was very quick, occurring over several days. Comparing the use of assumed QSA flows with the actual 1999 flows showed relatively small differences. Likewise the effect of clearer water made little difference. The development of such an intense and persistent stratification will have extreme and profound effects on the Sea. It will in all likelihood to the development of anoxia, which will in turn lead to the formation of H_2S and NH_4. There will be little opportunity for venting during the stratification period, so concentration will build up to unprecedented levels. The rapid breakdown of the stratification will lead to a sudden redistribution of anoxia, H_2S and NH_4 throughout the water column and to gaseous NH_3 and H_2S to the air. The effect of this will be an annual die off of all fish in the Sea, and potential human and wildlife mortality. While no other depths were examined, this result should be the same for all depths greater than 10 m. The half-Sea at 14 m depth had no days below 12°C.

The reason for this change in Sea behavior was shown to be the reduction in the production of turbulent kinetic energy due to shear production. This is a direct consequence of halving the length of the Sea. For the full-size Sea mixing is dominated by shear production (compared with wind stirring and convective overturn). For the half Sea this mechanism is largely eliminated. A dimensionless stability parameter (Lake Number) was calculated for both the full Sea nd the half-Sea. For the former, the value was always less than 2, and often less than 1 indicating very weak stability (i.e, propensity to mix). For the half-Sea the Lake Number was between 2 and 10 for most of the year, suggestive of a very stable water body.

1.0 Introduction

A one-dimensional hydrodynamic and thermodynamic model has been modified to evaluate the types of changes to the Salton Sea that might arise under scenarios that are currently under consideration by Reclamation. This model was the basis of DLM-WQ, which was recently used to model the eutrophic state of the current Salton Sea on behalf of the Regional Water Quality Control Board (Schladow et al. 2004). Whereas in the earlier study, the model included phosphorus cycling, sediment resuspension and algal growth the model used here eliminated these processes. The reasons for using the simpler model were two-fold. First, the time and budget available for the present study did not allow for the set up and running of the more complete water quality model. Second, there is insufficient information available about these processes in the Salton Sea under present conditions, let alone changed conditions in the future, to provide sufficient certainty for such a modeling exercise.

Instead, the approach taken was to model the thermal behavior of the Salton Sea. The processes that dictate the physical mixing of a water body and the thermodynamic exchanges at the air-water interface are well understood (see for example Fischer et al. 1979). Additionally, there exists a good meteorological data set at the Salton Sea, as well as several years of in-Sea temperature data to provide model validation.

The extent of thermal stratification under different Sea size configurations allows informed decisions about the likelihood and extent of water quality problems that are associated with thermal stratification. These water quality problems include hypoxia (low dissolved oxygen concentration), high H_2S concentration and high NH_4 concentration. All these conditions are detrimental to fish and invertebrate health in the Sea. Releases of gaseous H_2S and NH_3 increase the unpleasant odors at the Sea and could also have health effects on terrestrial animals, including the human population, if concentrations are sufficiently high.

2.0 Model Description

The UC Davis Dynamic Lake Model (DLM) is a one-dimensional model that simulates the vertical distribution of temperature and salinity in lakes and reservoirs. It is based on an earlier series of reservoir models developed at the Centre for Water Research (CWR) at the University of Western Australia (Imberger et al. 1978; Imberger and Patterson 1981; Hamilton and Schladow 1996). The assumption of one dimensionality means that variations in density, temperature, water quality parameters in the lateral directions are assumed to be small when compared with variations in vertical directions. The water quality version of the model, DLM-WQ, couples the transport and mixing processes to a set of biological and chemical processes that describe the growth of phytoplankton, the cycling of nutrients and the fate of particulate material.

2.1. Model Structure

The vertical profile of the lake is represented as a set of up to 150 Lagrangian layers, which are free to move vertically and to contract and expand in response to inflows, outflows, and surface-mass fluxes. The Lagrangian formulation avoids the need to calculate vertical velocities, greatly decreasing computational time and minimizing numerical diffusion, as compared with a fixed-grid Eulerian approach. Each layer is homogeneous, and property differences between layers represent the vertical distribution. Layer thickness is adjusted within the model according to the resolution required to represent the vertical density gradient. Density is calculated using the UNESCO equation for seawater, which is applicable up to a salinity of 45 parts per thousand. Although the Salton Sea has a different chemical composition to seawater, deviations in density are likely to be insignificant. The model is initialized with measured data for each layer.

Mixing is represented by the amalgamation of layers. Thus, for example, when wind mixing has produced sufficient turbulent kinetic energy to overcome the potential energy difference (density stratification) of the two upper layers, the two layers are simply combined. Properties of the amalgamated layer are volumetrically averaged, and the total number of model layers is decreased accordingly. Amalgamated layers may be split according to a specified maximum-layer thickness criterion, thereby maintaining the desired spatial resolution. Conversely, when a layer size falls below a specified minimum criterion, as may occur when there is withdrawal of water from the lake, then the layer is amalgamated with the smaller of the two bounding layers. Inflows are inserted at their level of neutral buoyancy after allowance for entrainment has been made. In the case of the Salton Sea, where the tributary flows are much fresher than the Sea water, the inflow spreads on the surface until it is mixed with the bulk of the surface layer.

2.1.1. Physical Processes Modeled

The basic model is constructed around five process descriptions, as described below. Additional processes (for example, sediment resuspension in the case of the Salton Sea model) are included as needed.

2.1.1.1. Surface Heat, Mass, and Momentum Exchange

The surface inputs of mass, heat, and momentum play a major role in determining the vertical distribution of properties in a water body. The model relies on the bulk aerodynamic formulae to calculate these transfers based on measured meteorological data. These are, for the stress τ, the sensible heat transfer H, and the evaporative heat transfer E:

$$\tau = \rho C_D U^2 \tag{2.1}$$

$$H = -\rho C_P C_H (T_A - T_S) \tag{2.2}$$

$$E = -\rho L_V C_W (q_A - q_S) \tag{2.3}$$

where U is the wind speed, T the air temperature, and q the specific humidity, with the subscript A referring to the air value, and S to the surface value. The coefficients C_D, C_H, and C_V are bulk aerodynamic transfer coefficients. C_P and L_V are the specific heat of water at constant pressure and the latent heat of evaporation of water respectively.

Radiative heat transfers are also an important component of the heat budget at the surface. The model considers short wave (wavelength 100 nm to 4000 nm), and long wave (wavelength greater than 4000 nm) radiation. Short wave radiation is usually measured directly, and the long wave LW_I either measured directly or estimated from cloud cover, air temperature, and humidity. Back radiation from the water surface is given by the Stefan-Boltzmann black body radiation law:

$$LW_O = \sigma T_K^4 \tag{2.4}$$

where T_K is the water temperature in ^oK, and σ is the Stefan-Boltzmann constant. Some of the incoming short wave radiation is reflected from the surface, with a reflection coefficient, or albedo, determined by the angle of the sun, the color of the water, or the state of the water surface. The shortwave radiation penetrates the water surface and is absorbed by the water column. In general, the absorption is determined by an attenuation coefficient which will depend on the wavelength and water clarity and color. In DLM, this absorption is often modeled by a Beer's Law formulation:

$$Q(z) = Q_O e^{-\eta z} \tag{2.5}$$

where Q_o is the radiation intensity at the surface, Q(z) the intensity at depth z, and η the attenuation coefficient. The attenuation coefficient may be related to the Secchi Disk depth d_S, as

$$\eta \sim \frac{1.7}{d_S} \tag{2.6}$$

In DLM-WQ it is related to the chlorophyll *a* concentration and a background attenuation coefficient (to allow for absorption by water and particle scattering). The long wave radiation is all absorbed in the first few mm of the water column.

In the context of the layer structure of DLM, the heat budget may be expressed as shown in Fig. 2.1. Only the top layer is affected by evaporative heat losses, sensible heat losses or gains, and long wave input and emission. Short wave radiation both enters and leaves the top layer, and provides a source of heat for lower layers, following Beer's Law.

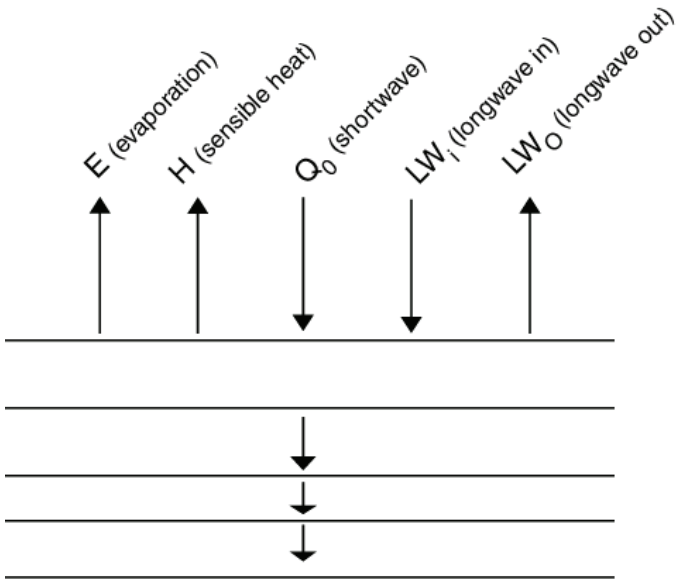

Figure 2.1—Schematic of heat flux through DLM layers.

If all of the fluxes are specified in units of Joules m^{-2} sec^{-1}, the net temperature increase of the top layer is given by:

$$\Delta T = \frac{[A_S(LW_I - LW_O - E - H + Q_O) - A_{S-1}Q_O e^{-\eta d_S}]\Delta t}{\rho V_S C_P} \qquad (2.7)$$

where A_S and A_{S-1} are the areas of the surface and penultimate layers, V_S is the surface layer volume, d_S is the upper layer thickness, and Δt is the time step in seconds.

The time step for the model is specified in the initial menu; in the case of the Salton Sea, a 2 hour timestep was found to be satisfactory.

After a single time step, the temperature structure will change as the result of the surface heat exchanges, as shown in Fig. 2.2. Note that after cooling, the surface layer is cooler than the underlying layer, an unstable configuration. This will be

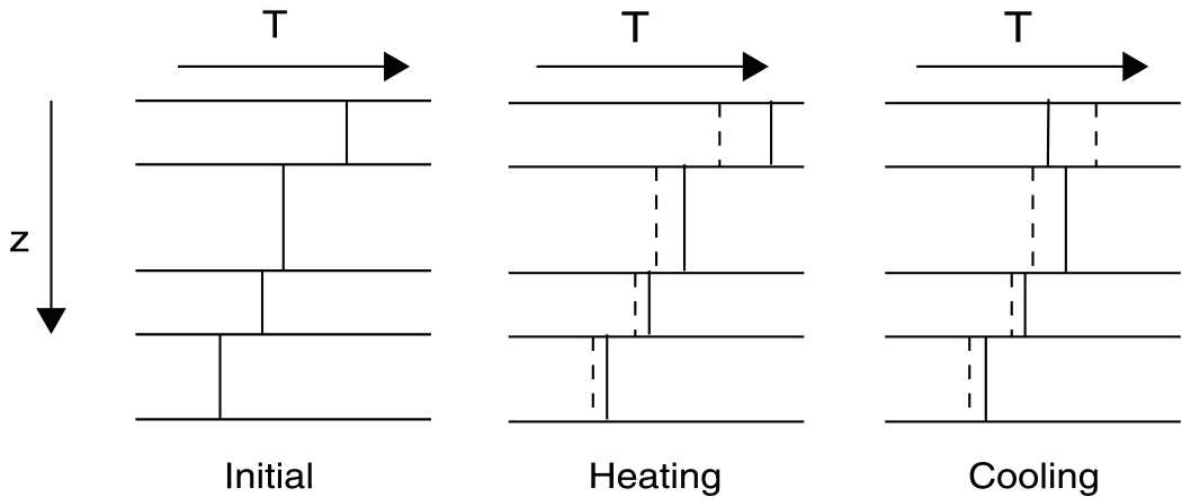

Figure 2.2.—Schematic of the effects of heating and cooling on layer stability.

dealt with by the mixed layer algorithm. The cooling profile shown also has sub-surface heating, corresponding to the absorption of shortwave radiation. Night cooling would leave the underlying layers unchanged.

The algorithm which describes the deepening of the surface layer is based on an integral model of the turbulent kinetic energy budget. Here, a certain fraction of the energy made available at the surface and at the interface between the mixed layer and the underlying water is made available to lift and accelerate the quiescent and relatively heavy water below the interface into the mixed layer. This may be achieved in several ways.

2.1.1.2. Convective Overturn

Cooling of the surface, as described above, leaves the temperature profile in an unstable state, with cooler water overlying warmer water. In reality, this cool, dense water will plunge in a turbulent plume, mixing with the water beneath. This process is modeled by a simple readjustment of the profile; that is, the surface layer density is compared with the density of the layer below and the two are mixed if gravitational instability exists. The resultant layer density is checked against the next layer, and the process repeated until the profile is stable, as shown in Fig. 2.3. In making this adjustment, the center of mass has been moved downwards, which implies that additional energy becomes available for further mixing. This may be expressed in terms of a velocity scale w_*. This energy is retained for the next process.

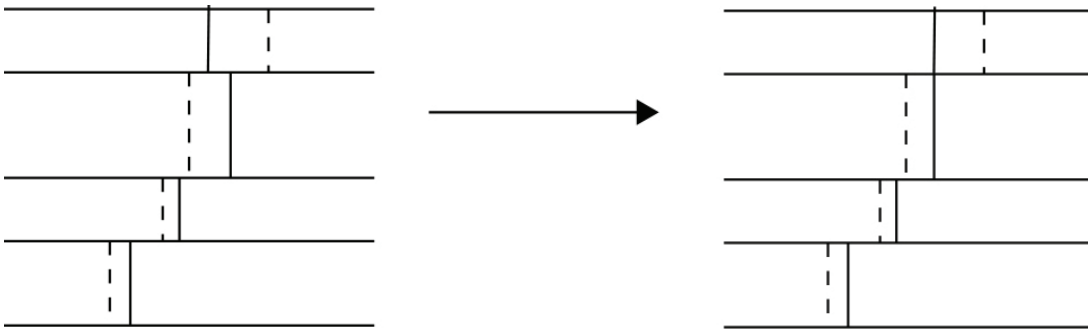

Figure 2.3.—Schematic of the effects of surface layer deepening by cooling.

2.1.1.3. Stirring

Some fraction of the energy input to the surface by the surface wind is available at the interface for mixing. The surface stress is given by

$$\tau = \rho_a C_D U^2 = \rho u_*^2 \tag{2.8}$$

which provides a means of calculating the energy input. The work per unit area by the wind is then

$$\tau u_* \Delta t = \rho u_*^3 \Delta t \tag{2.9}$$

The energy input from the convective overturn component discussed above may be included, to give

$$AKE = \frac{C_K}{2} \rho \left(w_*^3 + \eta^3 u_*^3 \right) \Delta t \tag{2.10}$$

where AKE is the available turbulent kinetic energy, η is a parameter which reflects the relative efficiencies of the convective overturn and wind stirring mechanisms, and C_K a parameter which reflects the efficiency of the stirring process relative to other processes.

2.1.1.4. Shear production

The action of the surface wind field, in addition to providing energy for deepening of the mixed layer, generates a shear velocity u_1 at the interface. As the interface

deepens through δh, conservation of momentum requires that the new shear velocity becomes

$$u_2 = \frac{hu_1}{h + \delta h} \tag{2.11}$$

In the change from u_1 to u_2, the total kinetic energy reduces by an amount

$$hu_1^2 - (h + \delta h)u_2^2 \tag{2.12}$$

where the small change in density is negligible. This energy becomes available for further mixing and is added into the AKE generated by stirring. Thus, the energy per unit mass is

$$AKE = \frac{C_K}{2}\left(w_*^3 + \eta^3 u_*^3\right)\Delta t + \frac{C_S}{2}u_1^2 \delta h \tag{2.13}$$

where C_S is a parameter which reflects the relative efficiency of the shear production mechanism.

To operate the shear production mechanism, a value for the shear velocity is required. This is obtained from the simple model:

$$\begin{aligned} u_1 &= \frac{u_*^2 t}{h} + u_{1_0} \qquad t < t_{eff} \\ &= 0 \qquad\qquad\quad t > t_{eff} \end{aligned} \tag{2.14}$$

where t_{eff} is the time beyond which shear production is no longer operative. The cut off time assumes use of only the energy produced by shear at the interface during the first wave period T_i, determined from the stratification, and modified to account for damping. The cut off time may extend beyond one model time step, and the wind stress may change over the period of t_{eff}. The cut-off time is directly related to the first mode internal wave period, which is proportional to the length of the water body. Thus, a reduction in length of a water body by say a factor of 2, will reduce the shear energy by a factor of 4 through Eqn 2.13, as well as reducing the time over which shear is acting, t_{eff}. As will be seen below, this will be a critical factor for the proposed changes at the Salton Sea.

The energy available for mixing, S, expressed as a rate of available energy AKE, is used to deepen the mixed layer. This means lifting relatively heavy water, and accelerating stationary water, both of which require energy. Thus the simplest mixed layer model balances the energy requirement with the available energy. Consider a mixed layer of depth h and density ρ0, with a density jump of Δρ at the base, which becomes mixed over a distance δh, as shown in Fig. 2.4.

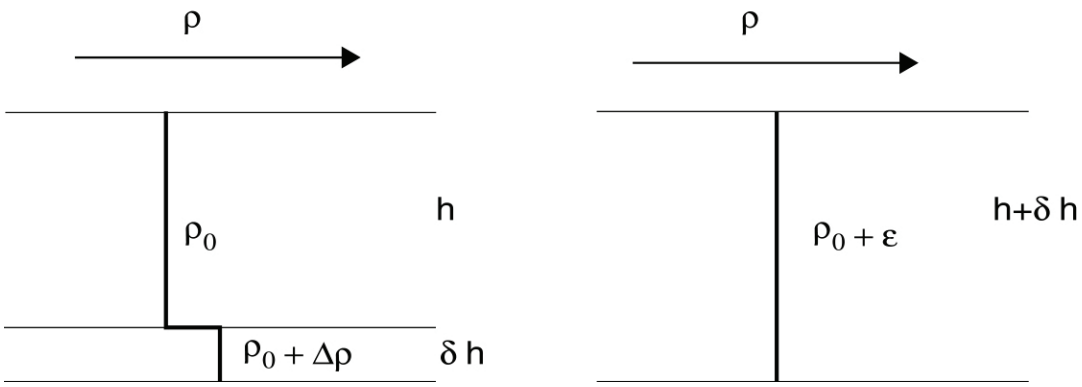

Figure 2.4.—Schematic of process of deepening.

The kinetic energy requirement is, therefore, $\frac{C_T}{2}\rho\left(w_*^3+\eta^3u_*^3\right)^{2/3}\delta h$.

The energy requirement per unit mass is therefore

$$SPE=\left[\frac{C_T}{2}\left(w_*^3+\eta^3u_*^3\right)^{2/3}+\frac{g\Delta\rho h}{2\rho_0}\right]\delta h \tag{2.15}$$

2.1.1.5. Billowing

The presence of shear at the interface may lead to a shear instability providing additional mixing. The effect of this is the formation of Kelvin-Helmholtz billows, which smear out the sharp interface generated by stirring and shear production. The scale of the billows is given by

$$\delta=\frac{0.3\rho_0u_1^2}{g\Delta\rho} \tag{2.16}$$

These provide both a source and a sink for energy, and therefore should appear on both sides of the energy balance.

$$AKE=\frac{C_K}{2}\left(w_*^3+\eta^3u_*^3\right)\Delta t+\frac{C_S}{2}\left[u_1^2+\frac{u_1^2d\delta}{6\,dh}+\frac{u_1\delta du_1}{3\,dh}\right]\delta h \tag{2.17}$$

$$SPE=\left[\frac{C_T}{2}\left(w_*^3+\eta^3u_*^3\right)^{2/3}+\frac{g\Delta\rho h}{2\rho_0}+\frac{g\delta^2\,d(\Delta\rho)}{24\rho_0\,dh}+\frac{g\Delta\rho\delta}{12\rho_0}\frac{d\delta}{dh}\right]\delta h \tag{2.18}$$

As noted above for shear production, the reduction in length of the water body by a factor of 2 will reduce δ by a factor of 4, thereby reducing the effectiveness of billowing in diffusing a sharp thermocline.

2.1.2 Energy Balance

In general, the balance between the available energy AKE and the required energy SPE provides an equation for the deepening rate dh/dt. In the context of DLM, where the time step Δt is determined elsewhere, and δh is constrained to be a layer thickness, the following procedure is followed, in simplified form. For each time step, the available energy AKE is calculated, based on the existing mixed layer of depth h, and w_* and u_* determined as above, after adjustment of the profile following surface cooling. The energy required SPE to mix in the next layer, of thickness δh and density $\rho_0+\Delta\rho$, is then calculated. If AKE > SPE, the layer is mixed, the mixed layer properties adjusted, AKE reduced by an amount SPE, and the next layer considered. If AKE < SPE, the energy AKE is not utilized, but is stored for use in the following time step. As the model takes each process in turn, the actual procedure is slightly more complex, but essentially follows the same path.

2.1.3. Mixing Below the Surface Layer

Mixing in the hypolimnion of lakes is patchy and sporadic, with individual events occupying relatively small volumes and occurring relatively quickly. However, in the context of all models of the DLM type, these events are modeled by a diffusive like process, with the actual events being parameterized by an eddy diffusivity K_z. The formulation in DLM follows the premise that the diffusivity depends on the dissipation of turbulent kinetic energy and inversely depends on the stratification. Thus:

$$K_z = \alpha \frac{\varepsilon}{N^2 + k_0^2 u^2} \tag{2.19}$$

where k_o is the wave number of the turbulent eddies, u the turbulent velocity scale, ε the dissipation, and α a constant related to the efficiency of the conversion of turbulent kinetic energy to mixing. In the hypolimnion, this diffusivity is applied to the diffusion equation, after calculation of ε, k_0 and u from the energy inputs of the wind.

3.0 Results

3.1 Model Validation

The model was initially run for a one year period using data from 1999 to verify that it matched the available measurements. Daily CIMIS meteorological data were used to drive the model. The Base Case condition used the measured average annual discharges. These were 620,000 acre-ft from Alamo River, 438,000 acre-ft from New River, 79,000 acre-ft from the Whitewater River and 106,000 acre-ft from agricultural drains (Schladow et al. 2004). The initial conditions were set based on measurements by Holdren and Montano (2002). A constant Secchi depth of 0.8 m was assumed. Time-depth temperature contours for the base-case and the measured data are shown in Fig. 3.1. Note that the measured temperature data were collected every 2-4 weeks, and at a few specific depths. By contrast the model output is daily, at a vertical resolution of approximately 0.1-0.2 m. As a result the measured data appear smoother than the modeled data.

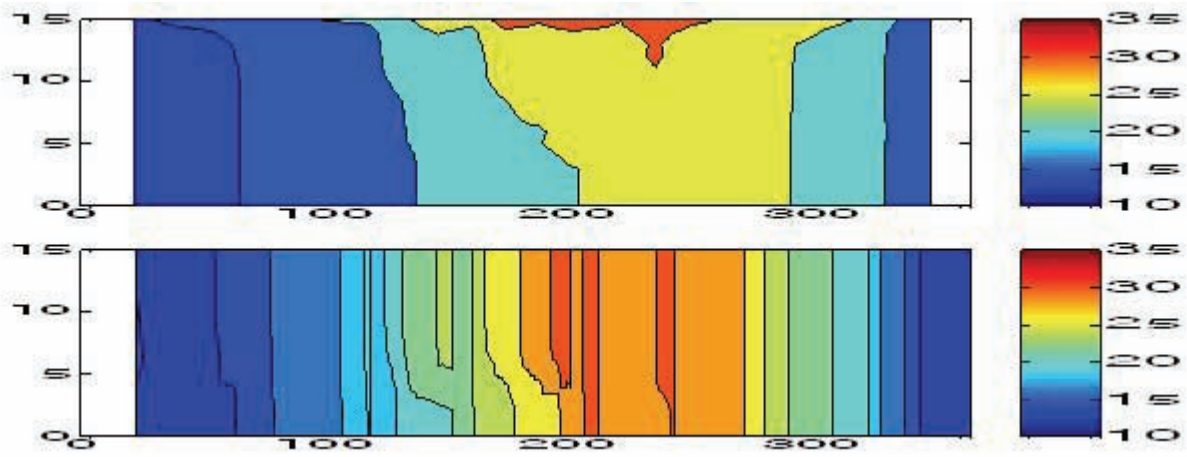

Figure 3.1—Measured (upper) and modeled (lower) time-depth temperature contours for 1999. Vertical axis is height above the bottom (m) and the horizontal axis is day of the year.

The results showed good agreement with the almost 12 months of measurements, particularly in light of the limitations stated above. The temperature distribution was characterized by stratification over an approximately 4 month period. The stratification was weak, broke and reformed several times, and was dominated by a broad thermocline. This is suggestive of the domination of shear mixing associated with seiching, and billowing. These processes would allow periodic venting of hypolimnetic water at the upwind end of the lake. This is consistent with satellite imagery and recorded fish kills associated with upwelling events in the past (Marti et al. 2005).

A second validation exercise was performed using two months of summer data from Cooke et al. (1998). Figure 3.2 shows the model result and the field data for temperature distribution in 1997. The data set extends from May 20 (day 140) to July 27 (Day 208) and includes the time when the Sea is stratified. The data set was from thermistors at elevations 1m, 7m, 11m and 12m from the bottom. There was no surface thermistor. This coarse instrument spacing (up to 6 m) and the interpolation required to produce contours, yields a somewhat smoother picture than the model result, which has a vertical resolution of 0.1 – 0.2 m. However, the overall trends agree very well. Both figures show a very broad thermocline initially, which finally breaks down between days 160 and 165. The weaker stratification that persists after that time, as well as the near-isothermy at the end of the period is picked up reasonable well by the model.

(a)

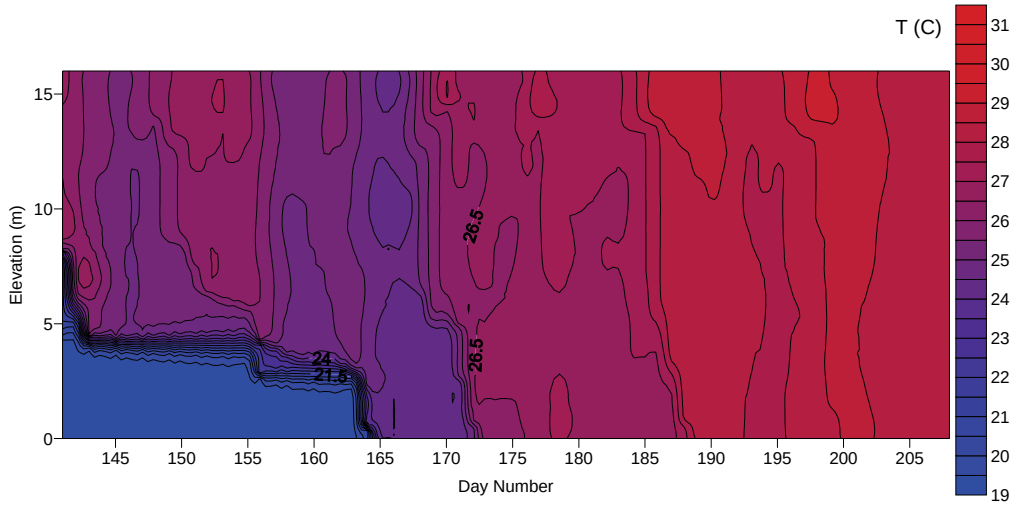

(b)

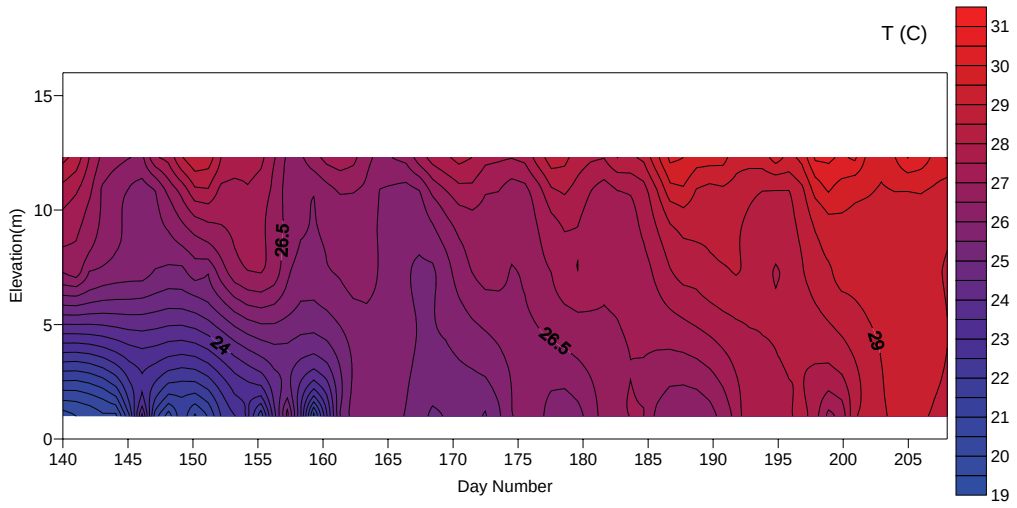

Figure 3.2.—(a) Measured temperature data from a station near the center of the Salton Sea (Cook et al., 1998). (b) Modeled temperature distribution using DLM.

3.2 Reduced Water Levels in a Full Sea

Two sets of simulations were run to examine the Sea's response under modified flow conditions. In both sets of simulations, the inflows to the Sea were assumed to be 800,000 ac-ft, evenly divided between the New and Alamo Rivers. The actual amount of flow in future years is highly uncertain, and the purpose of these simulations was not to look at the long term impacts of particular flows. Rather, it was intended to examine what the effect of a reduced Sea depth would be on the thermal stratification. These depths could be produced from any combination of future flows over many years,

The bathymetry of the Sea was preserved, but the initial water depth was altered. The 5 depths considered were 14.9 m (the base case from 1999 conditions), 14 m, 12 m, 10 m and 8 m. Meteorological conditions from 1999 were used to drive the one-year model runs. In addition the effect of the potential improvement in the eutrophication of the Sea was also examined. In the high clarity cases, Secchi depth was assumed to be 1.7 m, yielding an attenuation exponent of η=1.0 m-1. In the low clarity cases, Secchi depth was maintained at approximately current levels (SD = 0.8 m, attenuation η=2.1 m-1). The results are shown in Fig 3.3 and Fig. 3.4.

The results indicated that the 14.9 m and 14 m cases produced similar results. However for 12 m depth, only a very weak and short stratification period persisted. For the 10 m and 8 m cases, thermal stratification was virtually eliminated throughout the year. This implies that there would be very limited episodes of hypoxia and the production of H_2S and NH_4 for full Sea depths below 10-12 m. Model runs assuming a higher clarity Sea (i.e., less eutrophication) showed that stratification was slightly increased for the deeper Sea scenarios (14.9 m, 14 m and 12 m).

Figures 3.5 to 3.9 display the results in a slightly different way for each of the 5 depth cases considered. In each plot the upper panel shows the temperature of the warmest water in the Sea and the coldest water in the Sea for each day of the simulation. The middle panel shows the temperature difference for each day of the simulation. The occurrence of "cold water days" was also examined for each water depth (due to the impact on tilapia survival over winter). This is shown as a histogram of occurrence of water temperature below particular temperature ranges. For the 14.9 m and 14 m depths, there were no days with water temperatures below 12°C. Between 12 m and 8 m, the number of days with water temperatures below 10°C increased from approximately 15 to 25 days. The results shown are for the low clarity case only, as there was little difference with the high clarity case results. While low temperatures are considered to be a problemat for tilapia, salinity concentration associated with the shallower Sea levels would in all likelihood be beyond the survival range of tilapia.

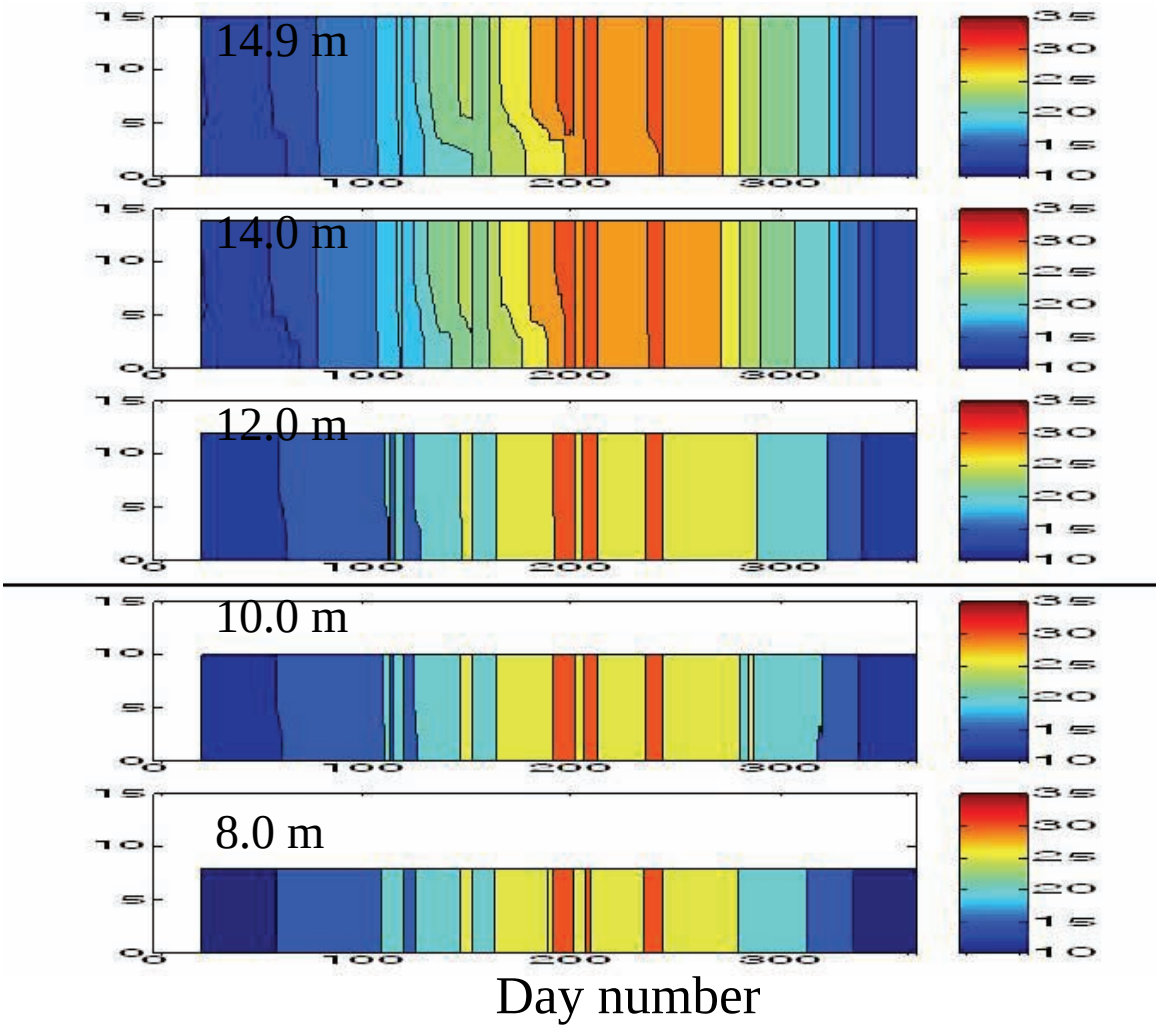

Figure 3.3.—Time-depth temperature contours for reduced inflow of 800,000 ac-ft with initial Sea depths of 14.9 m, 14 m, 12 m, 10 m and 8 m. High clarity case (SD = 1.7 m, attenuation η=1.0 m^{-1})

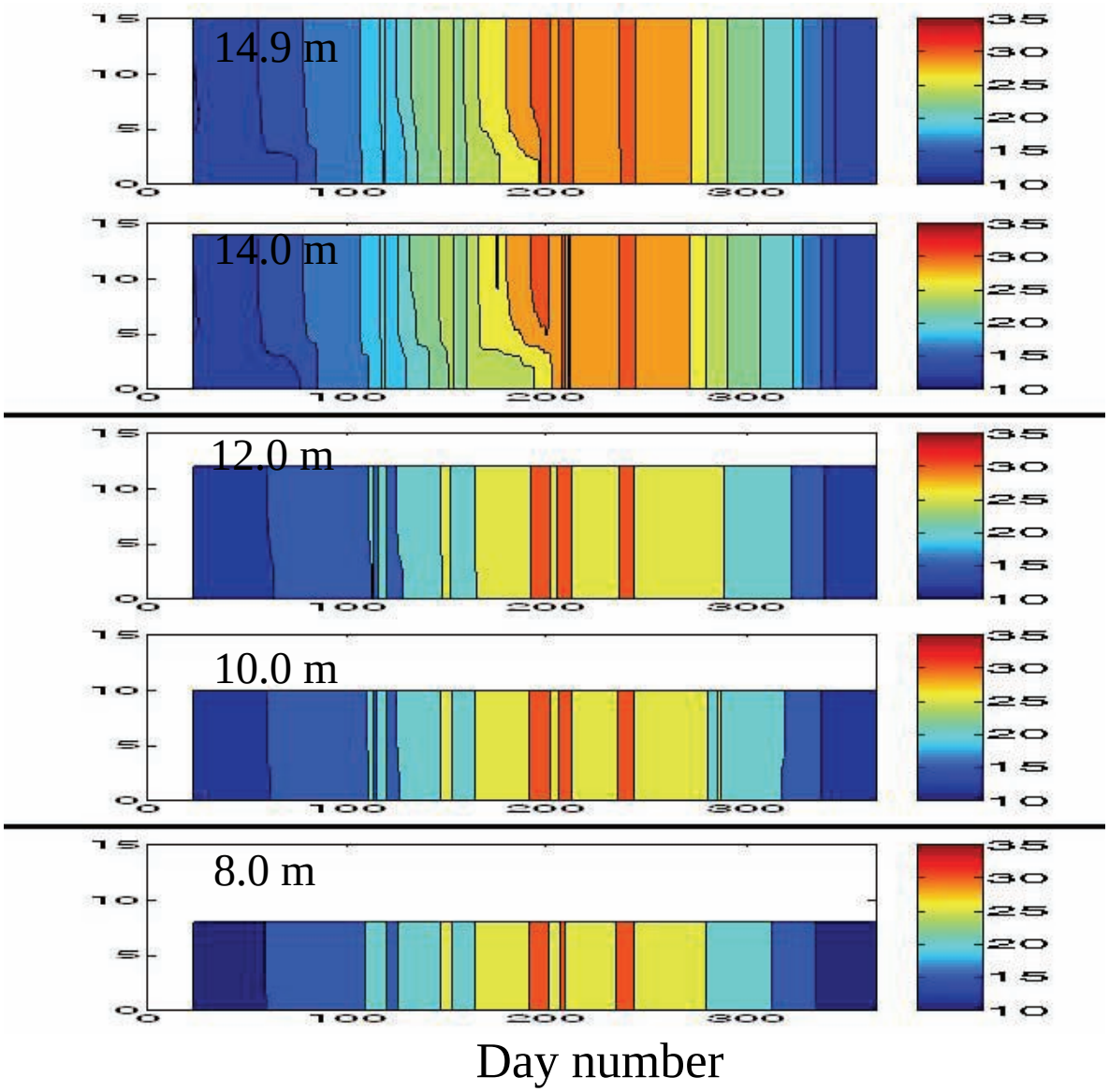

Figure 3.4.—Time-depth temperature contours for reduced inflow of 800,000 ac-ft with initial Sea depths of 14.9 m, 14 m, 12 m, 10 m and 8 m. Low clarity case (SD = 0.8 m, attenuation η=2.1 m^{-1})

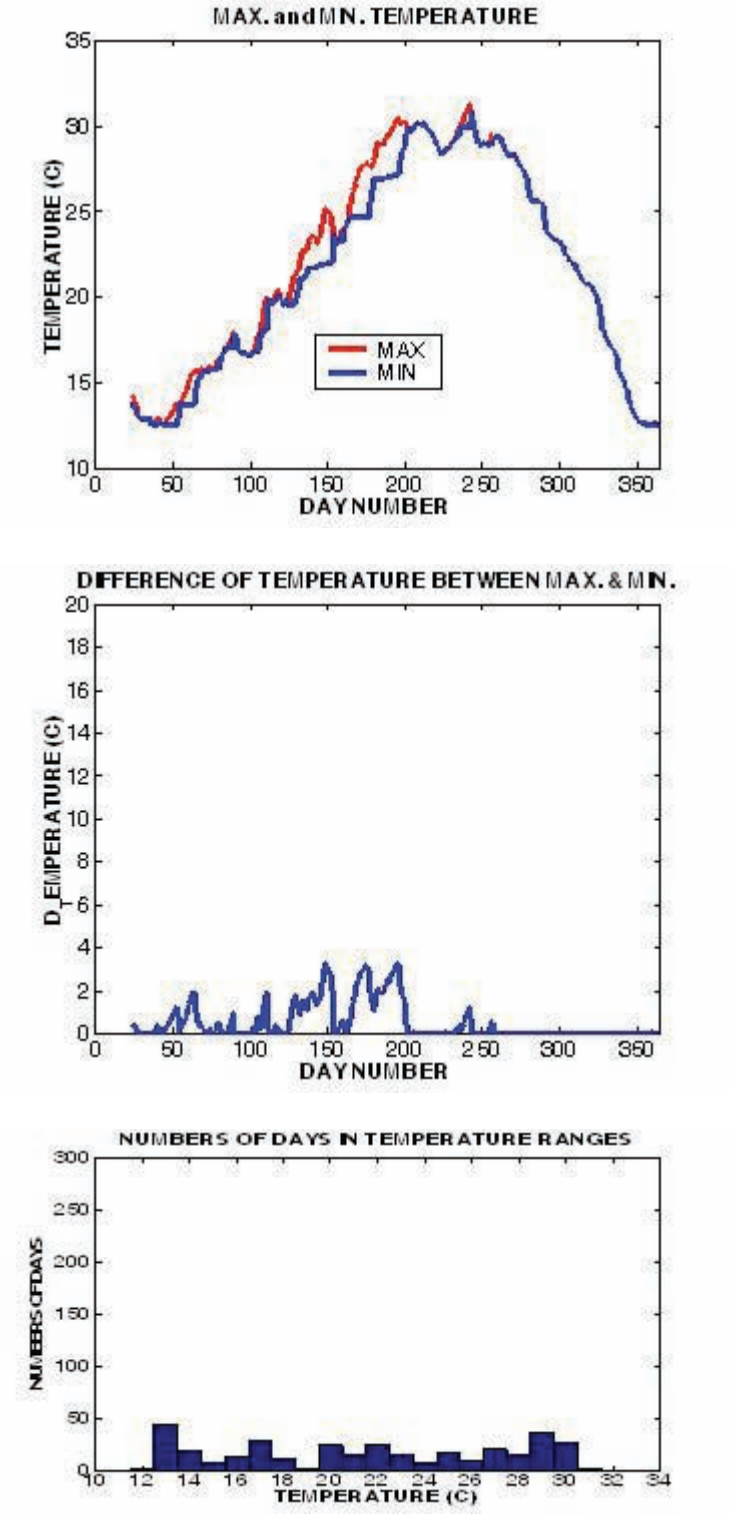

Figure 3.5.—14.9 m Sea with inflows of 800,000 ac-ft/year. Maximum and minimum temperature in the Sea for each day of the simulation (top panel); Temperature difference between the top and bottom of the Sea for each day of the simulation (middle panel); Number of days with temperatures falling below the range indicated (bottom panel).

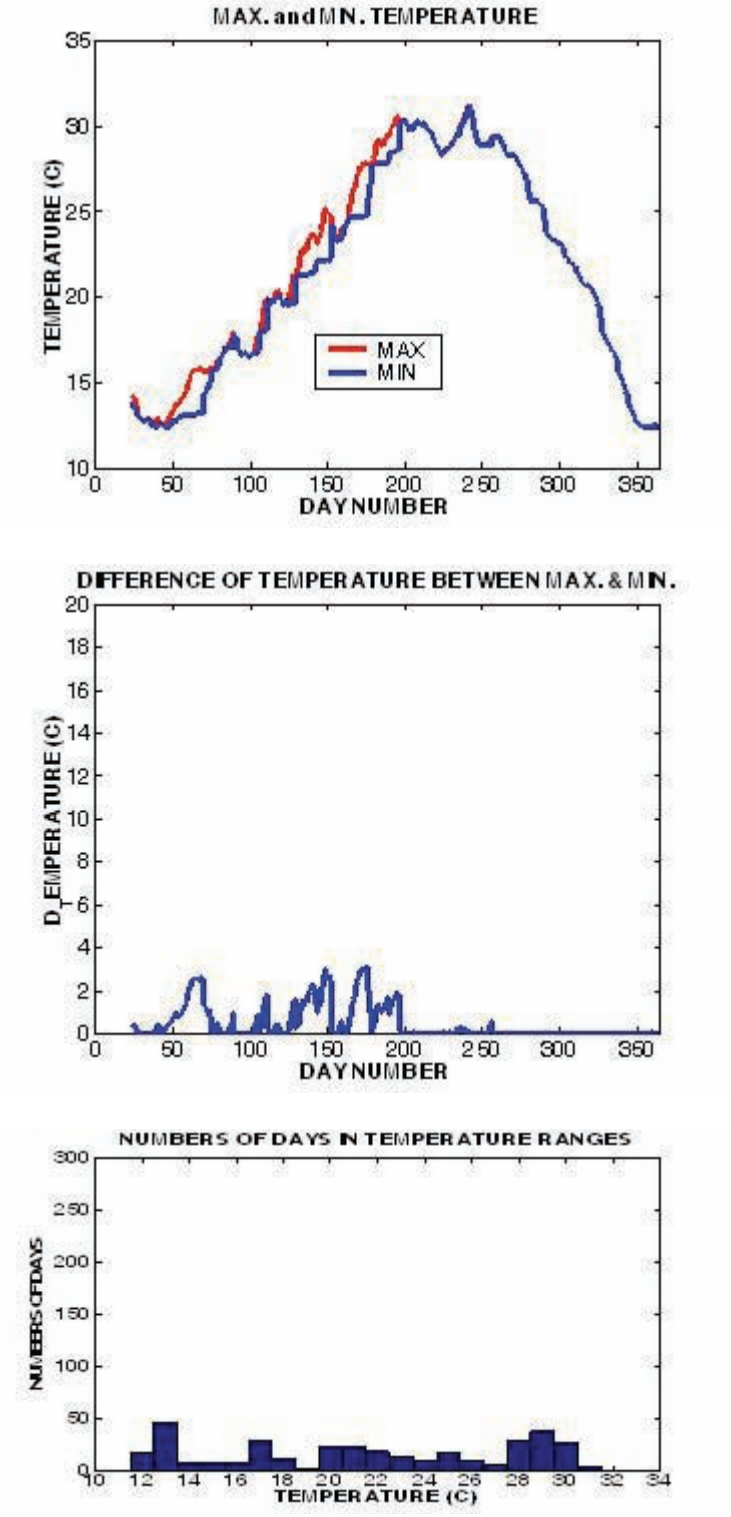

Figure 3.6.—14.0 m Sea with inflows of 800,000 ac-ft/year. Maximum and minimum temperature in the Sea for each day of the simulation (top panel); Temperature difference between the top and bottom of the Sea for each day of the simulation (middle panel); Number of days with temperatures falling below the range indicated (bottom panel).

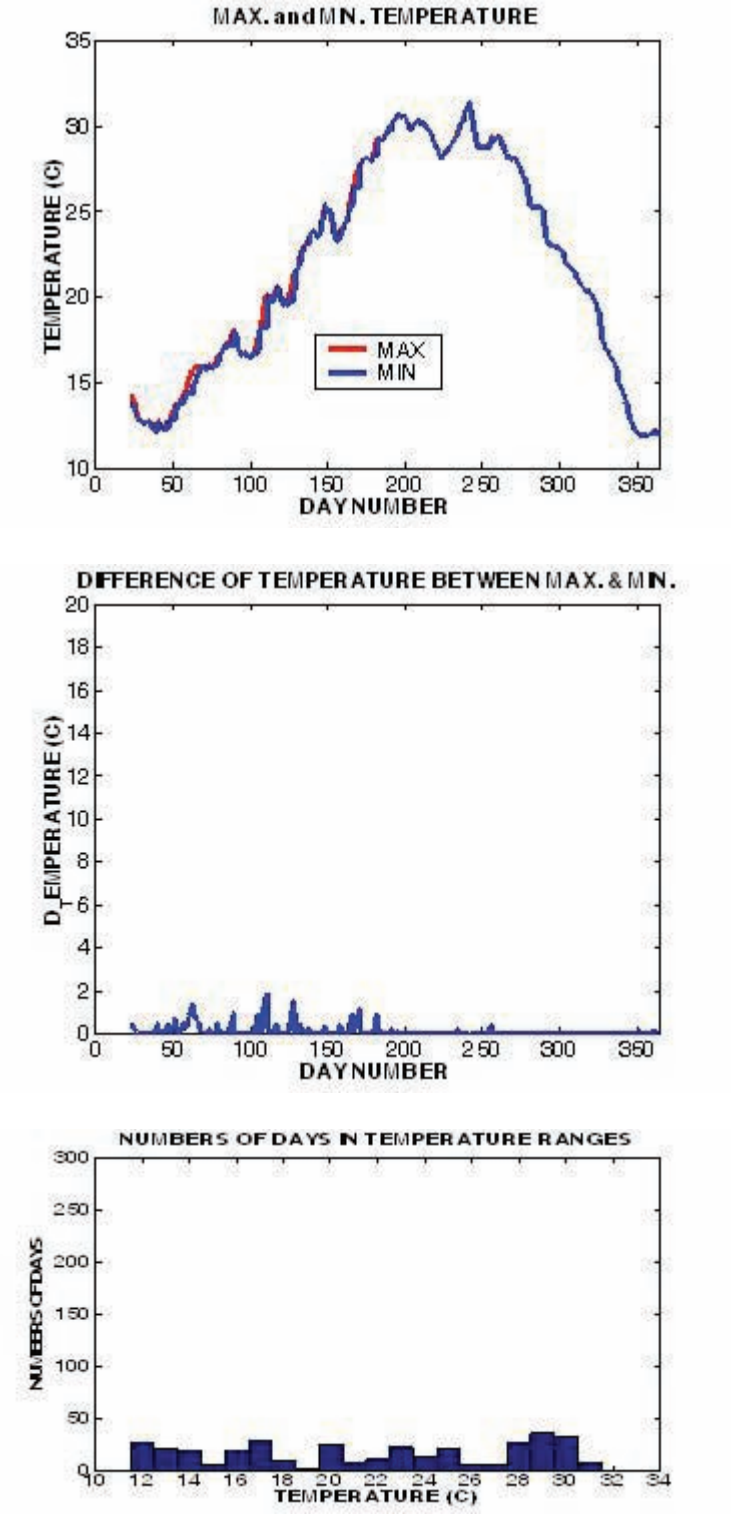

Figure 3.7.—12.0 m Sea with inflows of 800,000 ac-ft/year. Maximum and minimum temperature in the Sea for each day of the simulation (top panel); Temperature difference between the top and bottom of the Sea for each day of the simulation (middle panel); Number of days with temperatures falling below the range indicated (bottom panel).

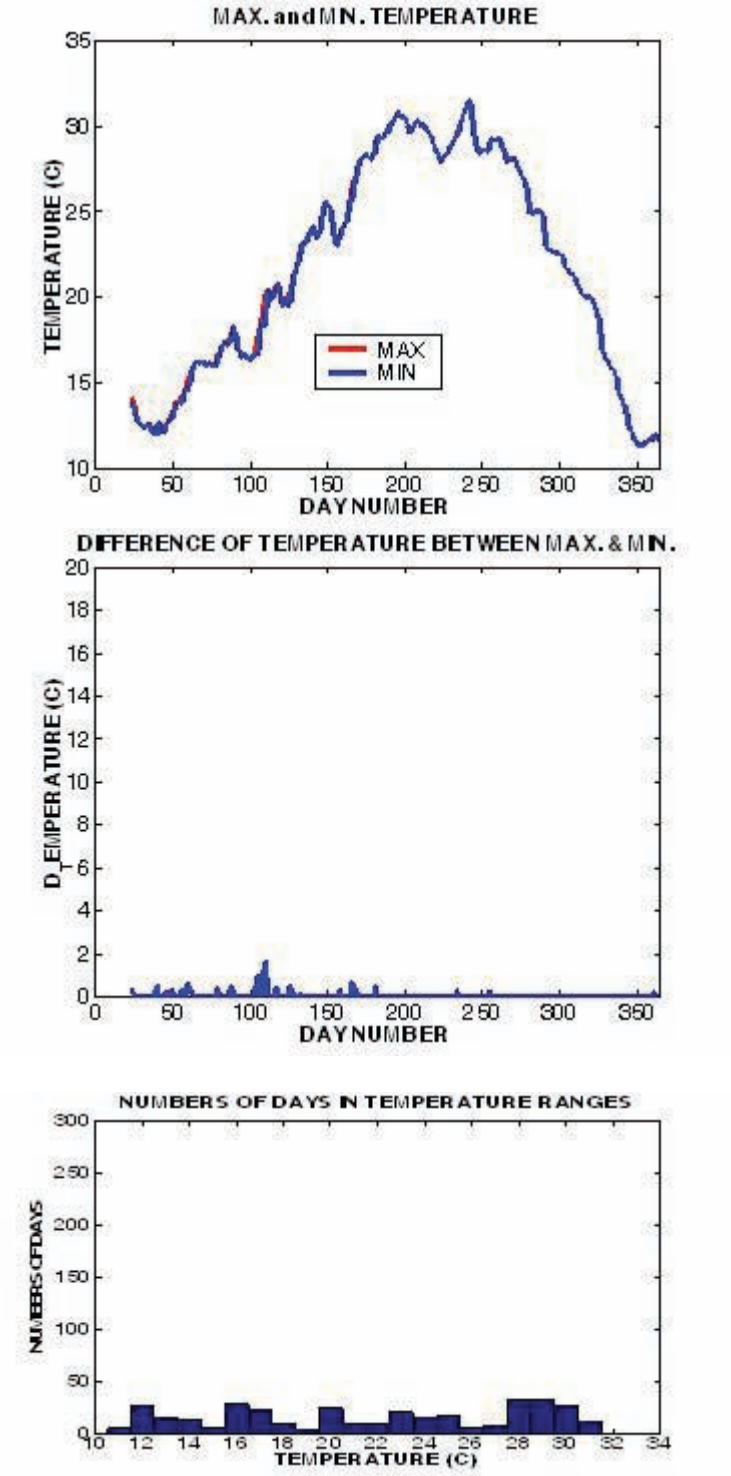

Figure 3.8.—10.0 m Sea with inflows of 800,000 ac-ft/year. Maximum and minimum temperature in the Sea for each day of the simulation (top panel); Temperature difference between the top and bottom of the Sea for each day of the simulation (middle panel); Number of days with temperatures falling below the range indicated (bottom panel).

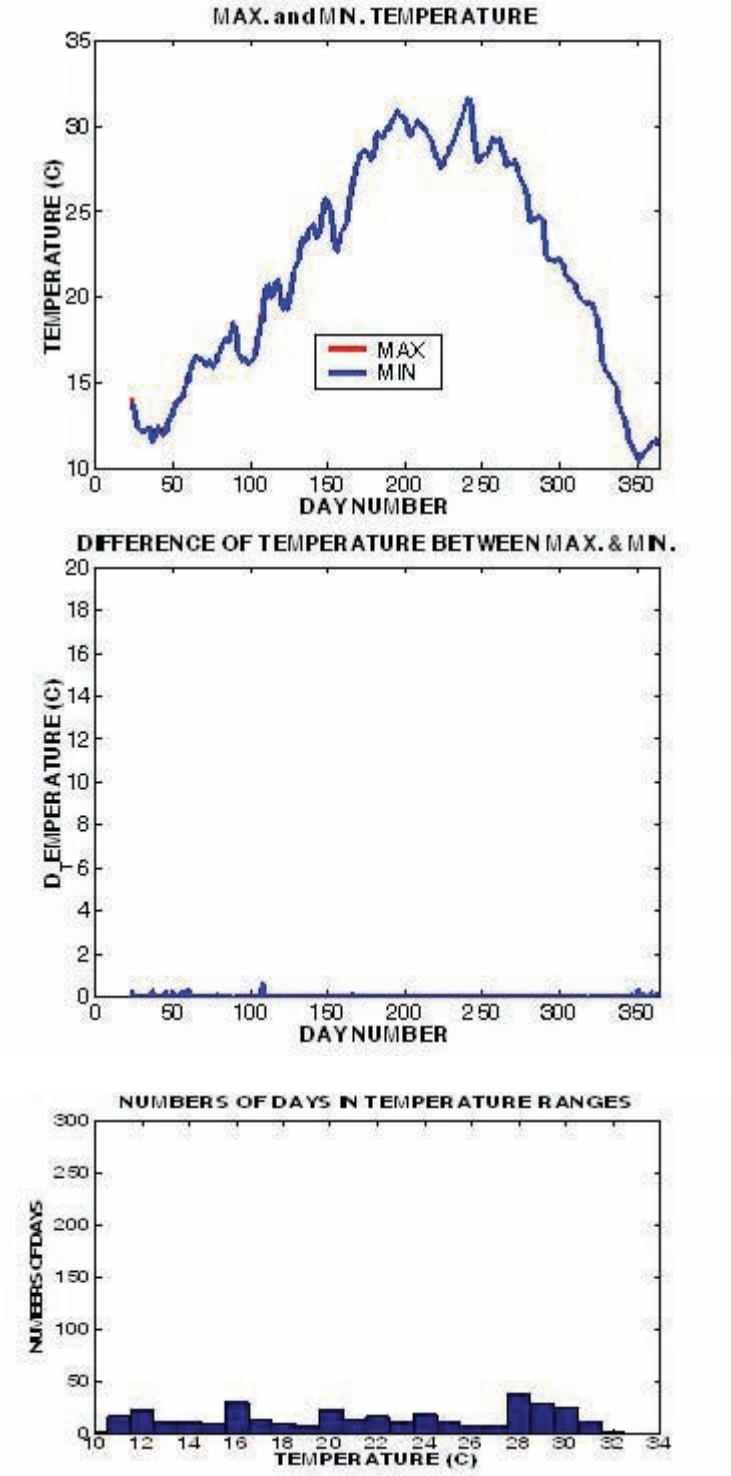

Figure 3.9.—8.0 m Sea with inflows of 800,000 ac-ft/year. Maximum and minimum temperature in the Sea for each day of the simulation (top panel); Temperature difference between the top and bottom of the Sea for each day of the simulation (middle panel); Number of days with temperatures falling below the range indicated (bottom panel).

Tables 3.1 and 3.2 present the number of days during the year when the Sea was not stratified for the low clarity and high clarity cases, for each of the depths considered.

Table 3.1—The number of days when the Salton Sea is not stratified (η=2.1)

Scenarios	Base	14 m	12 m	10 m	8 m
Non-stratification	206	227	311	333	341

Table 3.2—The number of days when the Salton Sea is not stratified (η=1.0)

Scenarios	Base	14 m	12 m	10 m	8 m
Non-stratification	206	227	311	333	341

Basically, with increasing clarity, the Sea becomes more homogenous in its temperature distribution (i.e., less stratified). The influence of clarity on stratification diminishes as the Sea becomes shallower.

3.3 Maintained Water Level in a Half-Sea

In a second set of simulations, the effect of dividing the Sea with a dam or barrier was explored. This was done by reducing the lake volume and area by 50% at all depths. While particular Reclamation scenarios differ from this, the effects of the differences between the various partial sea alternatives on the physics of the Sea are expected to be small for those alternatives that include a Sea with a depth close to that of the present Sea. The results are expected to be similar whether the remnant Sea is in the north or the south. A maximum Sea depth of 14 m was used for this set of simulations, assuming that the existing shoreline would be preserved.

The effect of halving the area of the Sea was dramatic, as shown in Fig 3.10 and 3.11. Figure 3.10 shows the time-depth temperature contours for both the non-QSA flows (assumed to be the 1999 flows described earlier and the QSA flows (assumed to be 800,000 acre-ft/yr). Thermal stratification was intensified in both cases, with the formation of a very sharp and intense thermocline commencing at a depth of about 4 m below the surface. The stratification was also extremely

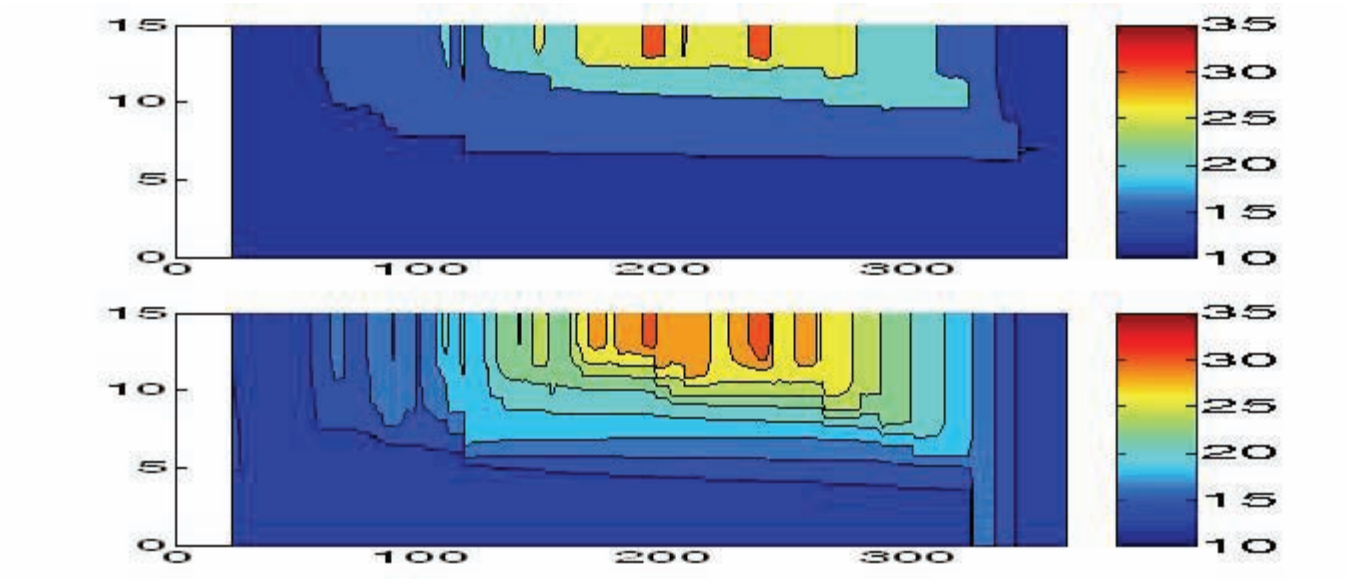

Figure 3.10.—Time-depth temperature contours for the Half-Sea under low clarity conditions (η=2.1) and with no QSA (upper panel). Time-depth temperature contours for the Half-Sea under low clarity conditions (η=2.1) and with QSA (lower panel).

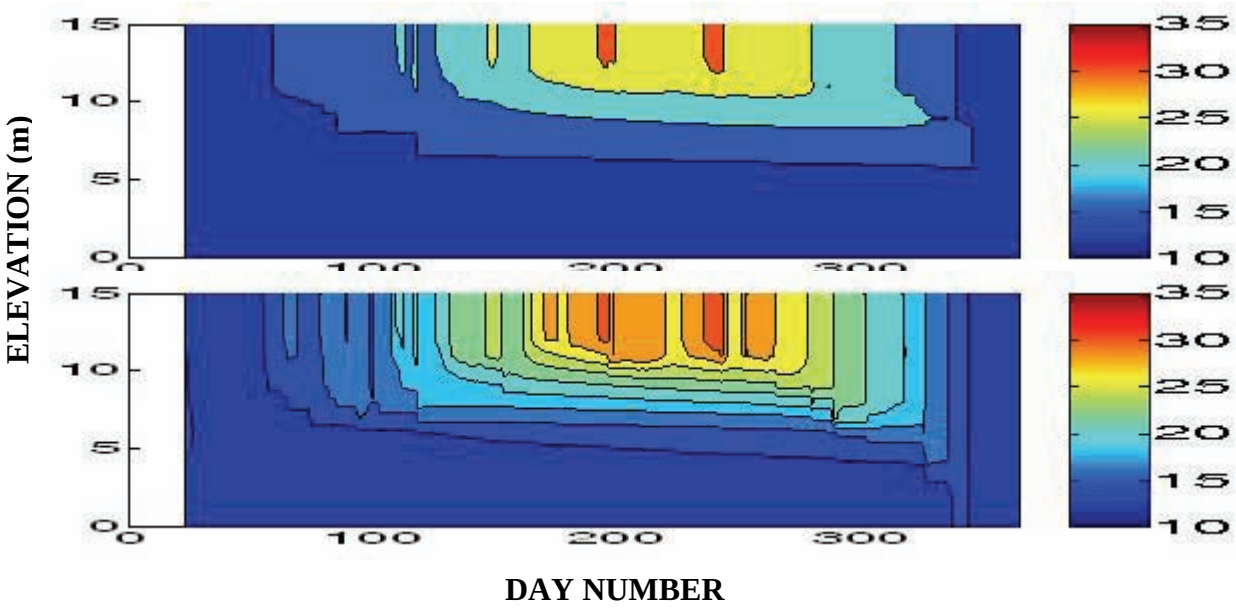

Figure 3.11.—Time-depth temperature contours for the Half-Sea under low clarity conditions (η=2.1) and with no QSA (upper panel). Time-depth temperature contours for the Half-Sea under low clarity conditions (η=2.1) and with QSA (lower panel).

persistent, with all but 1-2 months being stratified. Stratification was more intense for the QSA flows. The breakdown of stratification was very quick, occurring over several days. Comparing the use of assumed QSA flows with the actual 1999 flows showed relatively small differences. Likewise the effect of clearer water made little difference to the stratification.

Figure 3.12 shows the maximum and minimum water temperatures for each day of the simulation for all 4 cases. Note that the minimum temperature (the hypolimnetic temperature) remains consistently lower than for the simulations of the full sized Sea (Fig 3.5-3.9. The extent of the stratification is also clearly evident in these figures. Figure 3.13 shows the temperature difference between the surface and the hypolimnion of the Sea. Figure 3.14 shows the number of days with temperatures below a certain range.

The cases shown here are very different than the results for the full sized Sea. The strong stratification ensures that cool hypolimnetic temperatures are present throughout the year. This water is likely to be anoxic for most of the year. For the case of the low clarity Sea, the Sea is homogenous only 15 days without the QSA and 47 days with the QSA flows. This compares with 206 days for the full size Sea. For the high clarity Sea, the water column is homogeneous for 13 days without the QSA and 37 days with the QSA flows (compared to 265 days for the full sized Sea).

The reason for this change in Sea behavior was a reduction in the production of turbulent kinetic energy due to shear production. This is a direct consequence of halving the length of the Sea. For the full-size Sea mixing is dominated by shear production (compared with wind stirring and convective overturn). For the half Sea this mechanism is largely eliminated. Figure 3.15 shows the three main components of the turbulent kinetic energy (TKE) budget. The blue symbols show the TKE for the full size 14.9 m deep Sea, while the pink symbols are for the half-size 14.9 m deep Sea. The energy contributions due to wind stirring and convective overturn are almost identical for both cases. However, for shear production there is a marked decrease when the Sea is halved. It was formerly almost an order of magnitude greater than the other mechanisms.

A dimensionless stability parameter (Lake Number) was calculated for both the full Sea and the half-Sea. For the former, the value was always less than 2, and often less than 1 indicating very weak stability (i.e. propensity to mix). For the half-Sea the Lake Number was between 2 and 10 for most of the year, suggestive of a very stable water body.

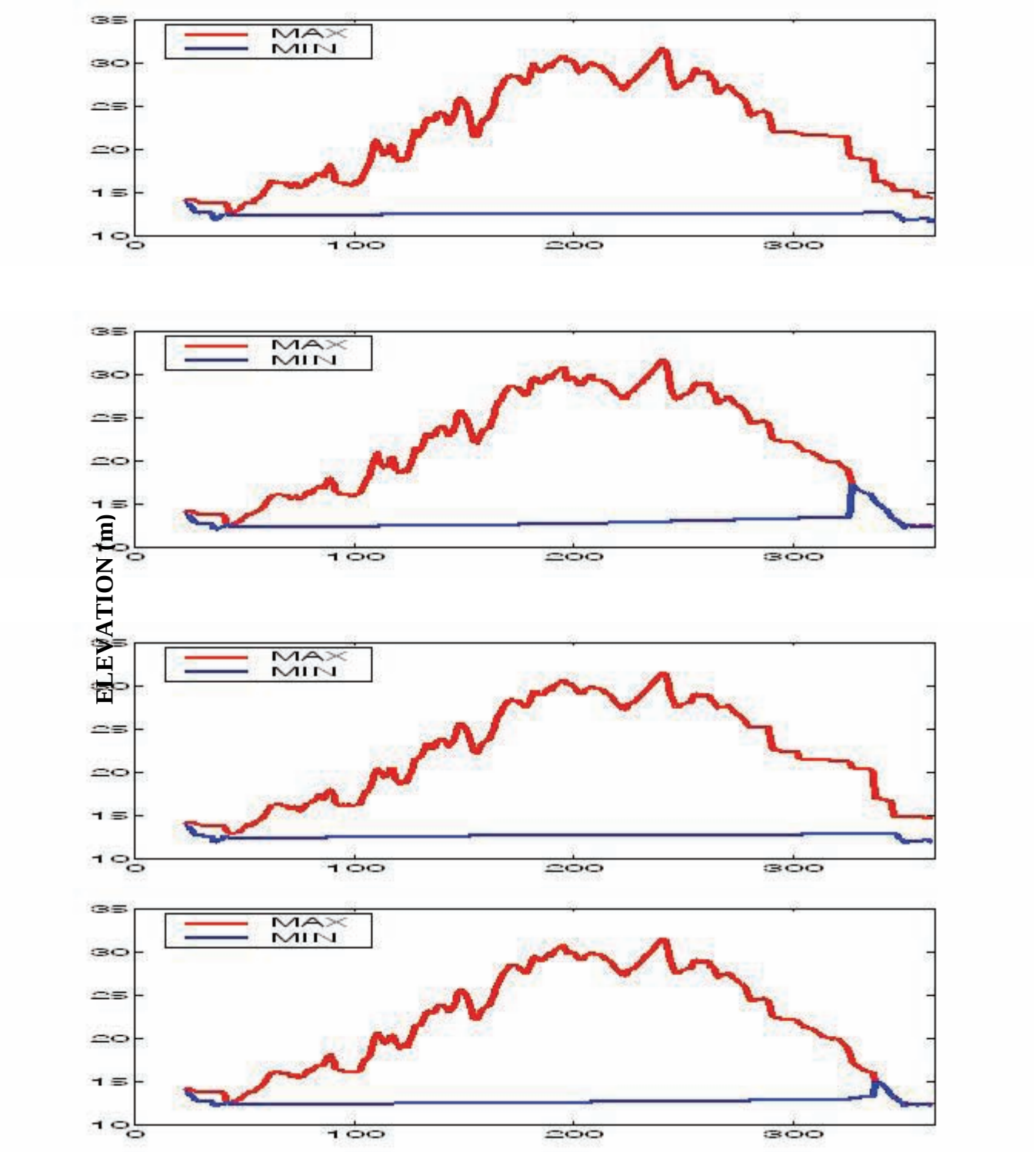

Figure 3.12.—Maximum and minimum temperature in the Sea for each day of the simulation . From top to bottom, the results are for: (a) no QSA, low clarity; QSA, low clarity; no QSA high clarity; QSA, high clarity.

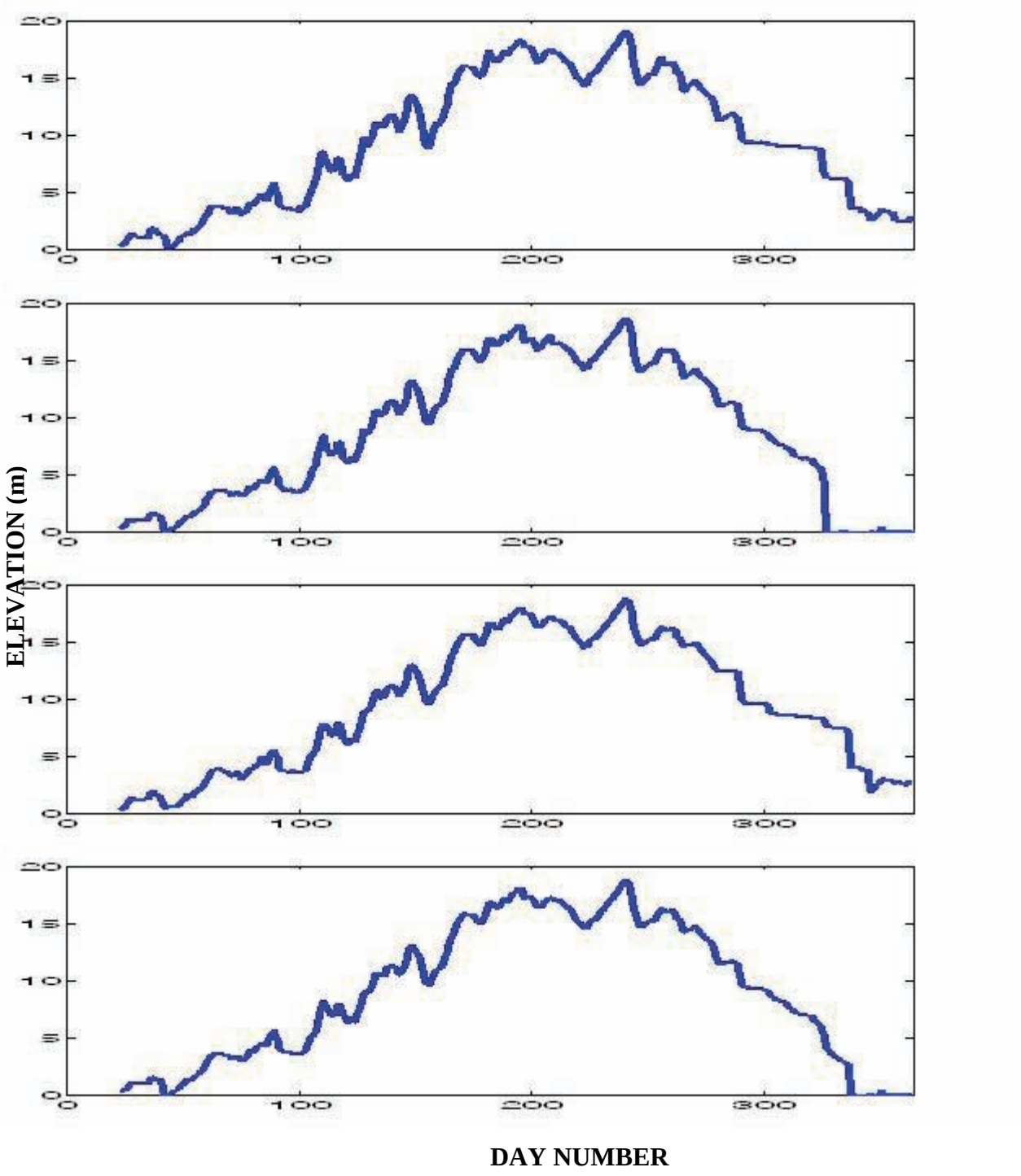

Figure 3.13.—Temperature difference top to bottom in the Sea for each day of the simulation. From top to bottom, the results are for: (a) no QSA, low clarity; QSA, low clarity; no QSA high clarity; QSA, high clarity.

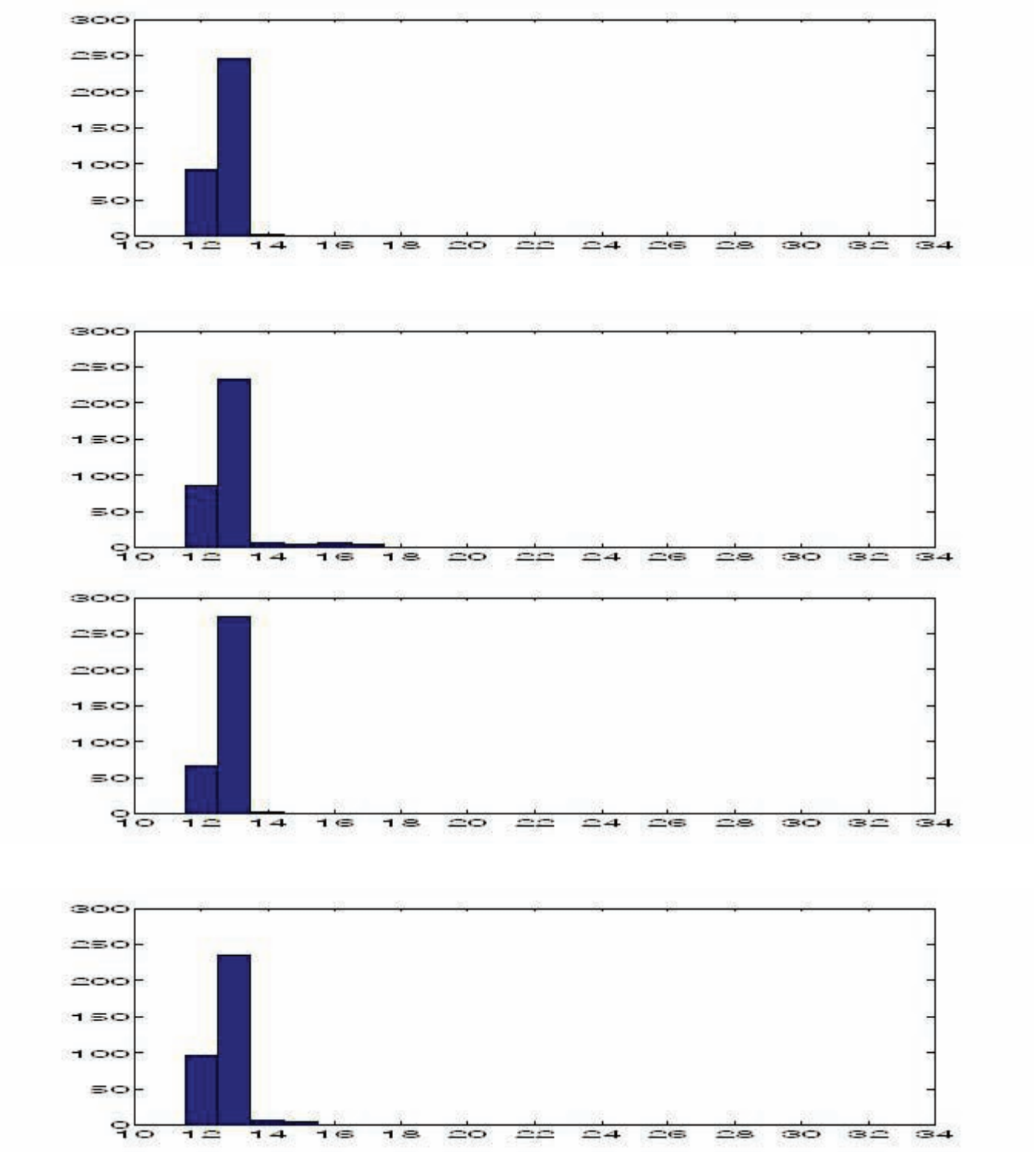

Figure 3.14.—Number of days with temperatures falling below the range indicated.

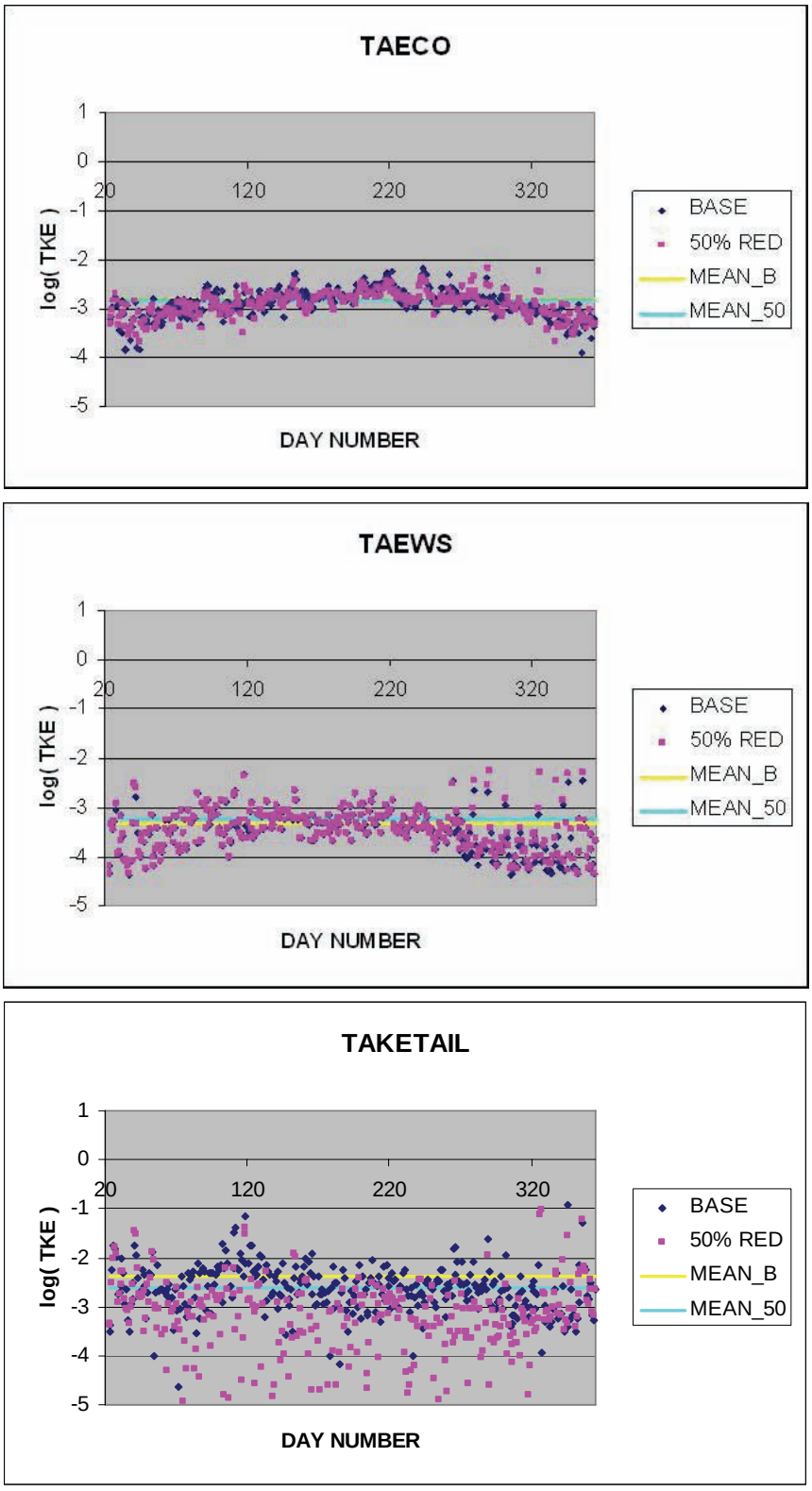

Figure 3.15.—Turbulent kinetic energy due to convective overturn (upper panel), wind stirring (middle panel) and shear production (lower panel) for the full sized Sea (BASE) and the half sized sea (50% RED).

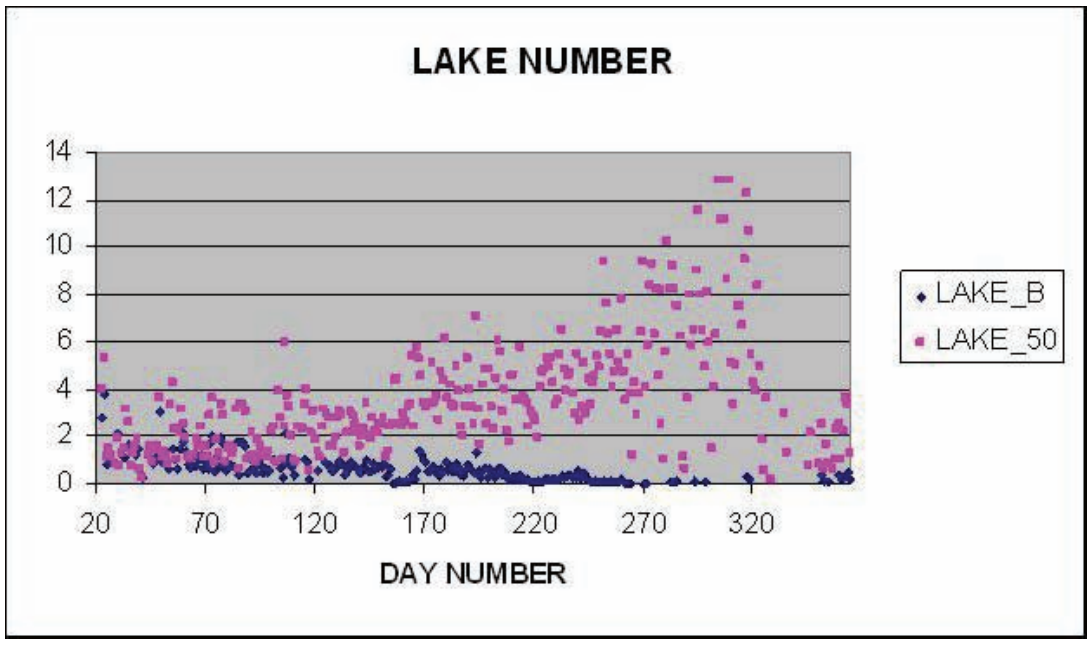

Figure 3.16.—Lake Number (calculated at 5 am daily) for the full sized Sea (LAKE_B) and the half sized Sea (LAKE_50).

4.0 Conclusions

The one-dimensional model, DLM, is capable of representing the vertical thermal structure of the Salton Sea. The results indicate that under current conditions (14.9 m maximum depth), the Sea is characterized by stratification over an approximately 4 month period. The stratification is weak, breaks and reforms several times, and is dominated by a broad thermocline.

For QSA flows of 800,000 ac-ft/yr results indicated that for 12 m depth, only a very weak and short stratification period persisted. For the 10 m and 8 m cases, thermal stratification was virtually eliminated throughout the year. This implies that there would be very limited episodes of hypoxia and the production of H_2S and NH4 for full Sea depths below 10-12 m. Model runs assuming a higher clarity Sea (i.e., less eutrophication) showed that stratification was reduced for the deeper Sea scenarios (14.9 m, 14 m and 12 m). As water depth decreases the minimum Sea temperature decreases. While this is dangerous for fish, the concomitant increase in salinity would eliminate fish from the Sea.

The effect of dividing the Sea with a dam or barrier was explored. This was done by reducing the lake volume and area by 50% at all depths. While particular Reclamation scenarios are a little different than this, the difference to the physics of the Sea are expected to be small. The results are expected to be similar

whether the remnant Sea was in the north or the south. A maximum Sea depth of 14 m was used for this set of simulations, assuming that the existing shoreline would be preserved.

Thermal stratification was intensified, with the formation of a very sharp and intense thermocline commencing at a depth of about 4 m below the surface. The stratification was also extremely persistent, with all but 1-2 months being stratified. The breakdown of stratification was very quick, occurring over several days. Comparing the use of assumed QSA flows with the actual 1999 flows showed relatively small differences. Likewise the effect of clearer water made little difference. The development of such an intense and persistent stratification will have extreme and profound effects on the Sea. It will in all likelihood to the development of anoxia, which will in turn lead to the formation of H_2S and NH_4. There will be little opportunity for venting during the stratification period, due to the high values of Lake Number, so concentration will build up to unprecedented levels. The rapid breakdown of the stratification will lead to a sudden redistribution of low dissolved oxygen, H_2S and NH_4 throughout the water column and the release of gaseous NH_3 and H_2S to the air. The effect of this will be an annual die off of all fish in the Sea, and potential human and wildlife mortality. While no other depths were examined, this result should be the same for all depths greater than 10 m. The half-Sea at 14 m depth had no days below 12 °C.

5.0 References

Hamilton, D.P. and S.G. Schladow. 1996. Prediction of Water Quality in Lakes and Reservoirs. Part I - Model Description. Ecol. Modeling, 96: 91-110.

Holdren, G.C. and A. Montano. 2002. Chemical and physical characteristics of the Salton Sea, California: Hydrobiologia v. 473, p 1- 21.

Imberger, J., J. Patterson, B. Hebbert and I. Loh 1978. Dynamics of reservoirs of medium size. J. Hydraul. Div., ASCE 104: 725-743.

Imberger, J. and J.C. Patterson 1981. A dynamic reservoir simulation model. DYRESM: 5. In: Transport models for inland and coastal waters. Ed. H. B. Fischer, pp 310-361. Academic Press, New York.

Marti, B., Steissberg, T.E., Hook, S.J. and Schladow, S.G. 2005. The mechanisms leading to fish kills in the Salton Sea as revealed by remote sensing. Salton Sea Symposium, San Diego, CA, Mar 2005.

Schladow, S.G. and D.P. Hamilton. 1996. Prediction of water quality in lakes and reservoirs. Part II - Application to Prospect Reservoir. Ecol Modeling 96: pp111-123.

Schladow, S.G., Robertson, D. M., Hook, S.J., Chung, E.G., Perez-Losada, J., Marti, B., Palmarsson, S. O., Steissberg, T. E. and Fleenor, W.E. 2004. Salton Sea Nutrients TMDL Modeling Studies. Draft Final Report. Submitted to: Colorado River Basin Regional Water Quality Control Board, 206 pp.